Environment International, Vol. 8, pp. 461-471, 1982
Printed in the USA.

0160-4120/82/070461-11$03.00/0

INDOOR AIR QUALITY MODELING: COMPARTMENTAL APPROACH WITH REACTIVE CHEMISTRY

H. Özkaynak
Energy and Environmental Policy Center, Harvard University, 140 Mt. Auburn Street, Cambridge, Massachusetts 02138, USA

P. B. Ryan, G. A. Allen, and W. A. Turner
Department of Environmental Health Sciences, Harvard School of Public Health, 665 Huntington Avenue, Boston, Massachusetts 02115, USA

Data on indoor/outdoor pollutant and tracer concentrations were collected during different periods in 1981 at a residence in Newton, MA. Special studies within the kitchen were conducted to determine the vertical and horizontal variability of pollutant and tracer gas concentrations. A reactive chemistry model incorporating simplified NO_x chemistry was developed to simulate pollutant concentrations indoors. Multicompartmental mathematical modeling tools were also developed and tested to estimate efficiently the effective, emission, ventilation, and removal rates, as well as the intercompartmental pollutant exchange coefficients. Model studies utilizing two- and three-compartment systems and tracer measurements proved that the dynamics of pollutant mixing inside a kitchen is not only complex but may be quite important in controlling spatial and temporal variability of reactive species. Further monitoring and modeling studies to investigate the critical aspects of the short-term dynamics of the reactive pollutants inside homes with gas cooking stoves are recommended.

Introduction

Most of the models developed for the purposes of predicting indoor air quality often fail to account for the temporal and spatial changes in the physical and chemical dynamics of the indoor environment. In particular, single-compartment indoor air pollution models utilizing solutions to the standard pollutant mass-balance equation commonly assume uniform or fixed values for mixing coefficients, pollutant transfer, transport, conversion, and removal rates. Under average or long-term (hour-day) modeling periods these assumptions are generally considered to be representative, but not, however, for the simulation of reactive species, such as O_3 and perhaps NO_x. Furthermore, this simplified approach poses serious limitations when modeling methods are needed to interpret or predict the behavior of peak pollutant concentrations or gradients, especially in homes with gas-fired stoves. From the point of estimating potential population health risks resulting from indoor exposures to various pollutants, it also becomes critical to understand the conditions and the time scales associated with the development of short-term, high-level (peak) exposures to reactive pollutants that may pose different health risks under (more acute) indoor exposure conditions than the conditions experienced outdoors.

In this work, we have attempted to study and address some of these technical concerns by developing alternative modeling options based on dynamic multicompartmental systems that are designed to simulate both the short- and the long-term reactive indoor pollutant profiles. The preliminary findings from our investigations reported here follow from a number of analysis and modeling activities that are based on (1) realistic compartmentalization of the source regions (e.g., kitchen) by multilayer components in the vertical and in the horizontal direction, (2) selection of representative transfer, source filtration, and removal rates based on actual measurements using numerical optimization tech-

niques applied directly to the multicompartment mass-balance equations, (3) incorporation of factors influencing the concentration profile of indoor pollutants, such as spatially and temporally varying intercompartment transfer coefficients, photolysis rates, deposition rates, and so on, and (4) provision to solve detailed chemical kinetics that may arise from the reactive nature of various indoor and outdoor pollutant species. The data base required to support the simulation and assessment work described here was obtained as part of a recent measurement program conducted in a residential home in Newton, MA.

Since the modeling requirements of this research placed strong emphasis on the accuracy and detail of short-term indoor/outdoor measurements, a significant portion of this work consisted of implementing new or sophisticated monitoring methods and data reporting protocols. Since the performance of this or any other modeling effort under similar circumstances will also depend on the quality and the resolution of the data sets generated, a brief description of the measurement protocol and equipment characteristics will be presented prior to proceeding with the development of the results for the multicompartmental simulations with reactive chemistry. Finally, it should be mentioned here that although the results presented are based on a limited number of measurements gathered in April and October 1981 from one house and thus may not be representative of other periods of construction types, the techniques used should be readily generalizable.

Description of the House and Its Ventilation Characteristics

The measurements were made in a single-family-occupied residence in Newton, MA, 11 km west of Boston. None of the residents smoke tobacco. The two-story plus full basement wood framed house, built in 1915, has aluminum siding, storm windows (on first floor), and a Gambrel roof. The first floor measures 8.2 × 9.3 m^2 and the kitchen measures 4 × 4.6 m^2, both with a 2.8 m ceiling. The second floor measures 9.1 × 7.3 m^2 with a 2.6 m ceiling. The home is approximately 30 m from a major highway. The first floor is elevated above the roadway by approximately 8 m. The heating system is forced hot water with a natural gas furnace located in the basement section. The furnace has pilotless ignition and an automatic flue damper. Both the furnace and the gas-fired hot water heater exhaust to a central brick chimney. All but two of the windows have storm panes which were closed during the time period of the measurements. Both first floor entrances are vestibule-type with storm doors, and there is a single basement door entrance. There is also a door separating the basement from the first floor. For the purposes of our modeling effort, the basement was not considered part of the dwelling, since the door between the first floor and the basement was always closed. There is no door separating the first floor from the second, just a large stairwell. There is an attic hatch in the ceiling of the second floor which was not sealed tightly.

Ventilation measurements were made several times before, after, and during the monitoring period using a manual SF_6 method. Measurements were carried out with a standardized procedure (Grot, 1979) using an SF_6 tracer gas and a model 505 "ITI Ion-Track Instruments" detector chromatograph. Maximum rates of 1.1 and 1.2 ach occurred with a moderate (approximately 10°C) indoor/outdoor temperature difference or during the operation of a kitchen exhaust hood. The minimum value measured was 0.3 ach on a warm calm day. The house could be classified as "rather leaky" and representative of much of the residential housing stock in the Boston area.

Description of the Monitoring System

Average values for CO, NO, NO_2, NO_x, and temperature were recorded for both indoors and outdoors in alternate 2-min intervals. Average stove gas flow, stove ventilation hood flow, and oven use status were recorded every 2 min.

Separate sample lines for CO and NO/NO_2 were run to the two sampling locations. The indoor sample was taken in the middle of the kitchen, 1.5 m above the floor. The outdoor sampling location was 2 m from the house, 1.7 m above the ground. Each line was a 7.6-m length of 3.2-mm FEP Teflon tubing, with a 5-μm particulate filter at the head of the line. A three-port Teflon solenoid valve was used to switch between the sample lines. All CO and NO/NO_2 spans and zeros were done through the entire sample train. Periodic span and zero checks through both lines were performed to insure the integrity of the sample train and the valve.

A Thermo Electron model 14 B/E single reaction chamber chemiluminescent $NO/NO_2/NO_x$ analyzer was modified to provide fast response and lower NO_2 skew error. The time for the modified analyzer to reach 95% of its final reading is 18 sec, including a 3-sec lag time. The time between NO and NO_x samples is 8 sec.

An Energetics Science series 2000 Ecolyzer was used for CO measurements. The analyzer was enclosed in a temperature-controlled box to eliminate drift due to changes in ambient temperature. A continuous duty AC pump was used in place of the standard DC sample pump. Only reaction cells that were in excellent condition were used, allowing a 95% response time of 20 sec, including the lag time of the instrument, the potassium permangenate NO interference filter, and the sample humidifier bottle.

Temperature was measured with type J thermocouple probes (Omega #ICSS-18G-4) mounted at the CO/NO_x sample probe locations. Stove gas flow was measured using a Teledyne Hastings-Raydist Mass Flowmeter

(model Nall-50k) with a full scale range of 50 L/min air. A correction factor of 0.69 for methane was used, making the effective full scale range 34.5 L/min.

The stove ventilation hood fan was triggered by a proportional delta T controller, with the sensors located at the hood inlet and 1.5 m to one side of the stove at the same height as the hood inlet. An approximate value for the hood air flow was recorded using a voltage that is proportional to the fan motor voltage. A calibration equation relating that voltage to the flow was developed by measuring the velocity of the air in the hood exhaust duct.

The oven status parameter (see Fig. 1) indicates oven use. (A mercury switch in the oven control knob is used to provide a signal whenever the knob is not at "off.")

Data were recorded with a Monitor Labs 9302 Data Logger and Techtran Data Cassette Recorder. This data logger also has the reference junction compensator and look up table for the thermocouples. Each parameter was sampled every 10 sec, along with a signal indicating the mode of the sample valve. An average value was recorded every two minutes. For the CO and NO/NO_2 monitors, data during the first 30 sec after a change in sample location were not included in the average value to allow the sample lines to flush and the analyzers to equilibrate. The combined response time of the analyzers and sample train were periodically checked to insure that the 95% response time of the system did not exceed 30 sec. A Texas Instruments TI-100 6 channel chart recorder was used as a backup data recording system for CO, NO, NO_2, NO_x stove gas flow, and stove hood flow. Oven status and valve mode signals were recorded on the event channels.

Throughout the monitoring period, a comprehensive quality assurance plan was followed. In addition to the system response time and sample valve checks mentioned above, a regular program of spans, zeros, multipoint calibrations, and internal audits was followed for the CO and NO/NO_2 analyzers. These quality assurance procedures were adapted from a procedure developed for the Harvard Six City Study Quality Assurance Manual. The mass flowmeter used for the stove gas flow was calibrated before and after the monitoring period. The thermocouple temperature system was periodically checked for accuracy.

In addition to the continuous NO_2 monitoring, 24-h integrated sampling was done in the kitchen using paired Palme's diffusion tubes and paired sodium arsenite bubblers. Weekly paired Palme's tubes were run outdoors, in the kitchen, and at two other locations indoors. Ver-

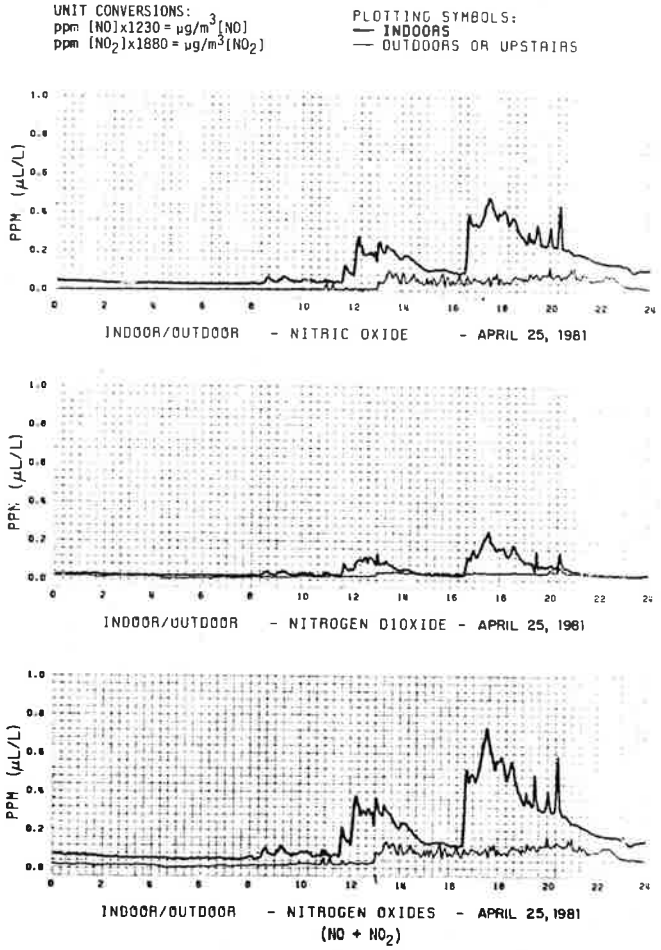

Fig. 1a. Indoor/Outdoor NO_x measurements, April 25, 1981.

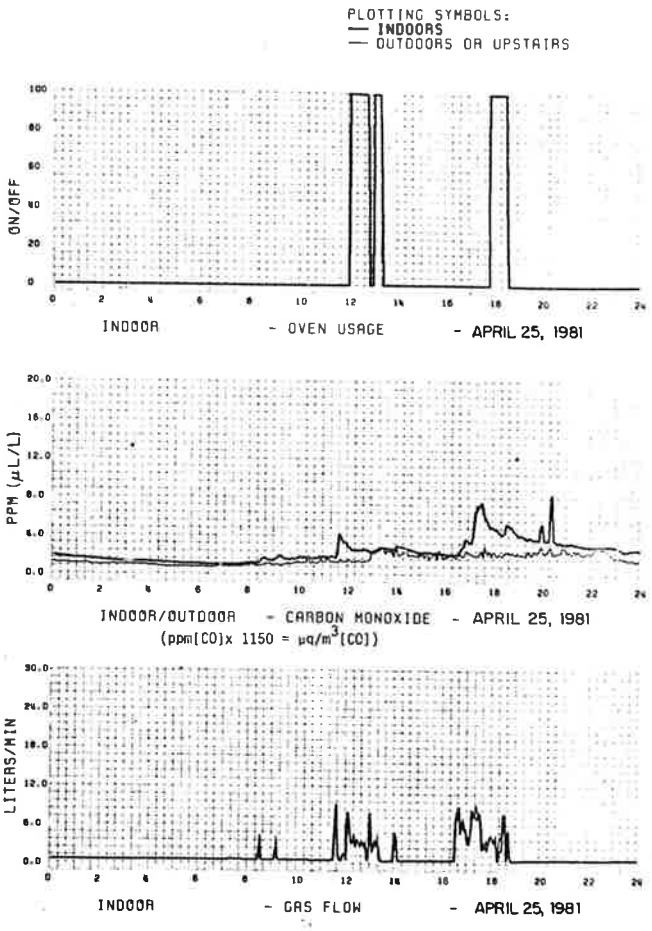

Fig. 1b. Indoor/outdoor CO, gas flow and oven usage measurements, April 25, 1981.

tical strings of paired Palme's tubes at 1-ft intervals were run for 1 week in the kitchen and the stairwell between the first and second floors. Results from these measurements, as well as a more detailed description of the monitoring instrumentation and an analysis of the indoor air data, will be published in the future.

Measurement Results and Model Applications

Data on pollutant and tracer concentrations were collected during April and May 1981 both inside and outside a residence in Newton, MA. Over this period, concentration profiles of key pollutant species such as NO, NO_2, and CO were monitored extensively. In addition, special studies were also conducted inside the kitchen to test the vertical and horizontal variability of concentration of these reactive species. Monitoring protocol was specifically developed in order to test the applicability of the well-mixed or one-compartment modeling hypothesis. (Figure 2 displays some of the multicompartment configurations that may be relevant within the kitchen or inside the house.) Our preliminary measurements in early 1981 had indicated that for short-term monitoring periods there may, in fact, be the potential for spatial concentration gradients inside the kitchen. To study in more detail the mixing properties within the kitchen, we conducted further tests during October 1981 by introducing instantaneous quantities of (SF_6) tracer gas above the center of the stove. These tracer experiments (discussed below) were performed both when the stove was off and when the stove was on.

The single and multicompartmental modeling techniques to be discussed here were principally developed for the purposes of characterizing and simulating the observed distribution of pollutants and tracers inside the kitchen.

In order to model the behavior of pollutant concentrations indoors, the following form of the mass balance equation was employed:

$$\frac{dC_j^i}{dt} = k_{jo}(C_o^i - C_j^i) + \sum_{l \neq j} k_{lj} C_l^i - \sum_{l \neq j} k_{jl} C_j^i + P_j^i - L_j^i, \quad (1)$$

where C_o^i = the outdoor concentration of pollutant species i ($i = 1,n$);
C_j^i = the indoor concentration of species i within compartment j ($j = 1,n$);
k_{lj}, k_{jl} = fractional exchange rates (transfer coefficients) between compartments l and j;
P_j^i, L_j^i = the (chemical) production and loss rates for the i^{th} pollutant species in compartment j.

The key assumptions inherent in the structure of Eq. (1) include the uniformity and diffusion free hypothesis characterizing the dynamics of the released pollutants.

Formulations such as these multicompartmental systems has been discussed in detail in NAS (1981). However, in the following we will report on theoretical development and applications utilizing similar models but that also include simplified NO_x chemistry. Methodology will also be presented to allow direct (one-step) estimates of key standard model parameters (such as ventilation rates, emission source strengths, heterogeneous deposition/chemical loss rates, etc.) using indoor/outdoor pollutant measurements and information on stove gas flow rates.

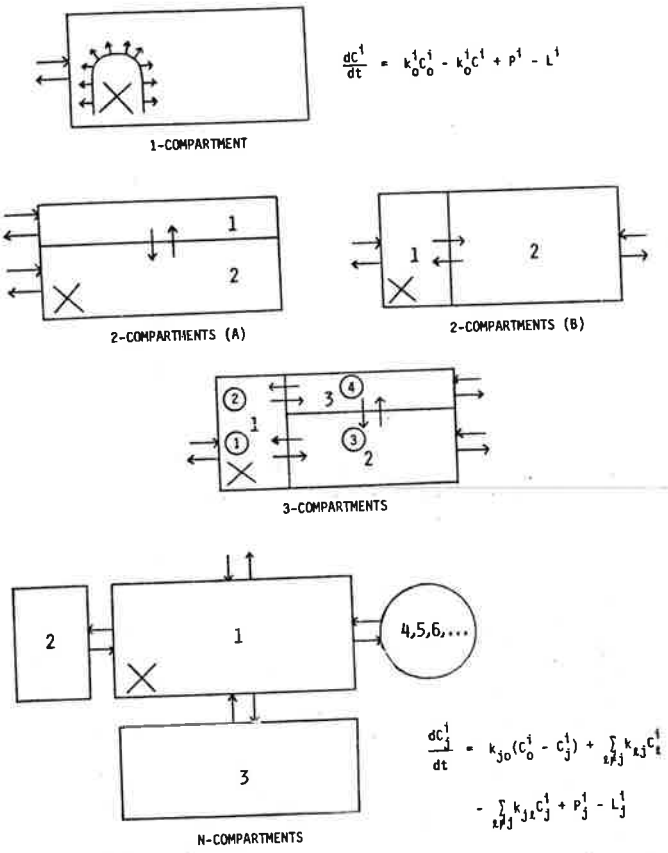

Fig. 2. Multicompartment systems pertinent to indoor air quality studies inside the kitchen or house (X describes the location of the gas stove and ①, ②, ③, ④ indicate the actual measurement points chosen inside the kitchen).

One-compartment simulations

The first-order mass-balance equation [Eq. (1) with $j = 1$] was initially used to model the observed change in measured pollutant concentrations. Since the comprehensive indoor/outdoor measurements conducted in April and May 1981 typically monitored concentrations at a fixed central position inside the kitchen, most of our modeling applications consisted of single-compartment studies. In the case of instantaneous releases of tracers or sources, it turns out that for measurement and simulation periods greater than 10–15 min following the

release of the source material, this well-mixed one-box assumption could be sufficient. However, as we will show later, especially during typical oven operation conditions (i.e., with continuous but variable pollutant emissions), the temporal profile of the peak and short-term pollutant concentrations inside the kitchen are highly dependent on the sampling locations. Nevertheless, the absence of mechanical ventilation, and the somewhat long averaging period simulated (greater than ~5 min), enabled us to develop and test a (one-compartment) simplified reactive chemistry model, as well as the modeling tools required to estimate various model parameters.

The role of reactive chemistry becomes important in the prediction of peak levels of certain pollutants. Indoor sources produce pollutants in nonequilibrium concentrations. Also, certain short-lived species are extremely reactive and affect the relative concentrations of important indoor pollutants such as NO and NO_2 in a very complex manner. It is with these considerations in mind that we decided to approach this problem in various stages of sophistication. Our initial efforts concentrated on constructing and applying a simplified but basic NO_x chemistry model.

The simplified NO_x chemistry was incorporated into Eq. (1) and into one-compartment species NO, NO_2, $O(^3P)$ and O_3 and their interaction in three reactions

$$NO_2 \xrightarrow{J_1} NO + O(^3P),$$

$$O_2 + O(^3P) + M \xrightarrow{k_1} O_3 + M,$$

$$NO + O_3 \xrightarrow{k_2} NO_2 + O_2. \qquad (2)$$

Molecular oxygen is not included as a chemical species in that its concentration is unaffected by this reaction scheme. This simplified chemical model accounts for most of the essential features of NO_x chemistry.

The single-compartment NO_x model can be summarized by:

$$\frac{dC^{in}}{dt} = P^{chem} - L^{chem} + R(C^{out} - C^{in}) - k_h C^{in} + S^{in}, \qquad (3)$$

where R = ventilation rate (min^{-1});
k_h = heterogeneous loss rate constant;
S^{in} = indoor source term.

This model accounts for:

- essential features of NO_x chemistry;
- infiltration and indoor sources;
- heterogeneous process:
  a. deposition;
  b. reaction with surfaces, e.g., walls, furniture, etc.;
  c. other pseudo-first-order reactions.

The assumptions made, however, include instantaneous mixing and steady-state approximation for $O(^3P)$ and O_3.

In the section below, using information on indoor-outdoor pollutant concentrations, model parameters necessary for the predictive indoor air quality simulations will be inferred by inverting the linearized form of Eq. (3) (mathematically this is defined as the inverse problem). In the subsequent section on reactive chemistry modeling, these inferred rates are used to generate the time dependent model estimates of (NO_x) pollutant concentrations (this is defined as the forward problem) to test the predictive capability of the techniques developed.

Estimation of model parameters

Descriptions of the time rate of change of the NO and NO_2 concentrations ([NO] and [NO_2]) are formulated using Eq. (3), as

$$\frac{d[NO]}{dt} = J_1[NO_2] - k_2[O_3][NO] + R([NO^o] - [NO]) - k_{h_1}[NO] + Q_{NO}, \qquad (4a)$$

$$\frac{d[NO_2]}{dt} = k_2[O_3][NO] - J_1[NO_2] + R([NO_2^o] - [NO_2]) - k_{h_2}[NO_2] + Q_{NO_2}, \qquad (4b)$$

where $[NO^o]$, $[NO_2^o]$ = the outdoor NO and NO_2 concentrations;
Q_{NO}, Q_{NO_2} = the NO and NO_2 emission rates;
[NO], [NO_2], [O_3] = the indoor NO, NO_2, and ozone concentrations, respectively;
J = the photolysis rate of NO_2;
k_2 = 25.2 $ppm^{-1}\ min^{-1}$ [0.013 $(\mu g/m^3)^{-1}\ min^{-1}$];
R = the ventilation (filtration) rate;
k_{h_1}, k_{h_2} = the heterogeneous rate constants for NO and NO_2, respectively.

A common technique used in solving Eqs. (4a) and (4b) involves explicit integration to provide analytical solutions to this system of equations. This direct approach, however, often becomes limited when more than a few reactive pollutant species are modeled through the coupled kinetics. Under these (also more realistic) conditions, numerical integration of Eq. (4) by forward finite difference methods (as discussed in the following

section) enables real-time prediction of concentration profiles. To be able to perform such (forward) simulations, knowledge of various reaction, exchange, deposition, ventilation rates, and so on, is essential. The most direct and mathematically justified methods of estimating these rate coefficients [which are the k parameters in Eq. (4)] is to invert directly the mass balance equation after appropriate linearizations are performed. The method employed (cf. Özkaynak *et al.*, 1982 for details) relies principally on numerically solving the constrained least-squares-regularization problem:

$$\min_{I \geq 0} \left\{ \|D - AK\|^2 + \lambda \|K\|^2 + \gamma \|K - H\|^2 \right\}, \quad (5)$$

where K = the vector of inferred J, $k_2[O_3]$, R, k_{h_1}, k_{h_2}, Q_{NO}, and Q_{NO_2} values;
D = the rate of change of pollutants minus the gas flow rates;
A = the matrix (or weighted kernel) representing coefficients of the linearized pollutant balance Eqs. (4a) and (4b);
γ, H = the equality constraint coefficient and arrays, respectively;
λ = the regularization parameter that is adjusted to control measurement errors and mathematical ill-conditioning resulting from the inversion of the associated Fredholm equation of the first kind.

Put differently, this optimization process (i.e., estimations using linear programming techniques) provides non-negative, thus physical, rate estimates, that minimize the sum of square of differences between the observed and the predicted (concentration based) data values, while at the same time satisfying a number of prespecified requirements that pertain to the overall distribution and uniformity of the magnitude of solutions, as well as to the accuracy by which filtration rate estimates are weighted relative to those of Q_{NO} and Q_{NO_2} estimates.

Non-negative least-squares algorithms developed by Lawson and Hanson (1974), along with the Tikhonov (1963) regularization formulation, were applied during this investigation (cf. Özkaynak *et al.*, 1982 for further details) to demonstrate the utility of such an approach in estimating at one step all of the unknown physical parameters, such as filtration, mixing, intercompartment transfer, and removal rates. Ultimately, the recovered rates are supplied as inputs to the simple reactive chemistry model described below to compute the time dependent pollutant concentration predictions.

Mathematical inversion of the unknown rate constants were implemented over 2-h periods (i.e., assuming fixed rate constants over this length of time) using the optimization algorithms described above with matrices, D and A computed using the discretized pollutant measurements and gas flow rates (similar to information shown in Fig. 1). Results of these recoveries are shown in Table 1. Altogether, there were 7 separate days that were modeled during this phase of the study. Only two of those cases included the "stove on" simulations. Therefore, the recoveries were typically effected without the source terms Q_{NO} and Q_{NO_2}. Estimation of the source terms Q_{NO} and Q_{NO_2} were generated using the prespecified (in effect, implemented by the equality constraints γ and H) ventilation rates as determined separately by the five parameter optimizations using the decay part of the NO_x curves beginning right after the stove was turned off (e.g., April 24/14 simulation incorporated the value of the inferred filtration rate from "stove off" April 24/16 simulation).

Associated with each inferred value displayed in Table 1 there are varying degrees of uncertainties or errors. Typically J_1 and k_{h_2} estimates have the largest uncertainties due to inherent numerical formulation difficulties with errors in the range of ±50% (see also the following section). The other parameters are typically

Table 1. Estimated values.[a]

Date/Time[b]	J_1(min^{-1})	$[O_3]$(ppb)	R(h^{-1})	k_{h_1}(h^{-1})	k_{h_2}(h^{-1})	Q_{NO}(ppm/L)	Q_{NO_2}(ppm/L)
April 24/14[c]	0.002	0.00	0.3	0.22	0.20	0.0001	0.0006
April 24/16	0.010	0.14	0.3	0.27	0.1	–	–
April 25/14	0.002	0.02	0.4	0.15	0.5	–	–
April 25/16[c]	0.0006	0.0	0.3	0.04	0.16	0.0004	0.0003
April 25/18	0.0003	0.04	0.2	0.02	0.5	–	–
April 26/12	0.017	0.02	0.4	0.07	0.2	–	–
April 26/20	0.016	0.30	0.2	0.06	0.4	–	–

[a] Unit conversions: ppb$[O_3]$ × 1.96 = $\mu g/m^3[O_3]$;

$$\frac{\text{ppm}}{\text{L}} Q_{NO} \times 1230 = \frac{\mu g/m^3}{\text{L}} Q_{NO};$$

$$\frac{\text{ppm}}{\text{L}} Q_{NO_2} \times 1880 = \frac{\mu g/m^3}{\text{L}} Q_{NO_2};$$

ppm = $\mu L/L$;
ppb = $\mu L/m^3$.

[b] Recoveries represent 2-h average values approximately starting from the hour of day indicated.
[c] Simulations represent stove and/or oven on conditions.

6.

expected to be within ±20%–40% of those estimates shown in this table. (These error bounds are obtained by examining many recoveries that yield similar residual and solution norms when the regularization parameter λ is varied between 0.1 to 100. (See AER, 1981 for more details.)

Comparison of the observed versus inferred values suggest that the recoveries are quite reasonable and satisfactory. Not surprisingly, the NO_2 photolysis rate, J_1, is smaller than that expected for outdoor. (Outdoor values are typically in the range 0–0.4 min^{-1}, from Williams *et al.*, 1980.) Inferred O_3 values were somewhat small. But later direct ozone measurements conducted in October supported our estimated values [during this later experiment indoor ozone values were measured to be less than 0.5 ppb ($\mu L/m^3$) at instrument detection limit]. Ventilation rates determined were also consistent with our SF_6 measurements. Finally, NO and NO_2 emission rates were found to vary in the 2 days studied. However, the magnitude of our estimated Q_{NO} and Q_{NO_2} values and the phenomenon of the variability of relative NO and NO_2 source strengths (from one day to another) were also consistent with the findings of Traynor *et al.* (1981).

Reactive Chemistry Modeling

The simple reactive chemistry scheme given above [Eq. (2)] accounts for the essential features of NO_x chemistry in the indoor environment. It has been established (NAS, 1981) that the concentrations of both NO and NO_2 are present in elevated levels indoors when compared with outdoor concentrations. This is especially true in dwellings equipped with gas stoves. These levels are still quite small when compared to concentrations of molecular oxygen so that this species concentration remains unaffected by this reaction scheme.

The rate constants k_1 and k_2 are those measured experimentally for the production of ozone and oxidation of NO to NO_2, respectively (Whitten *et al.*, 1980). The photolysis rate for destruction of NO_2, J_1, has been inferred from the data using the techniques outlined in the previous section. The photolysis rate so determined falls in a range consistent with values measured outdoors, at ground level (Bottenheim and Strausz, 1980). As might be expected, the values inferred are lower than the outdoor values, an effect consistent with lack of direct sunlight in the indoor environment.

The (forward) predictive model consists of first determining the rate of change in species concentration at the current time:

$$\frac{dC_{ii}^l}{dt} = P_i^l - L_i^l + (C_{io}^l - C_{ii}^l)R - k_{hi}C_{ii}^l + S_i^l,$$

where C_{ii}^l = concentration of the ith species indoors at time step l;
C_{io}^l = concentration of the ith species outdoors at time step l;
R = infiltration/exfiltration rate;
k_{hi} = heterogeneous rate constant for species i;
S_i^l = source of species i at time step l indoors;
P_i^l = chemical production of species i at time step l;
L_i^l = chemical loss of species i at time step l;

The concentration at the next time step is then given by explicit first order finite difference approximation:

$$C_i^{l+1} = C_i^l + \tau \frac{dC_i^l}{dt}, \quad (6)$$

where τ is the time increment.

In this study, we have attempted to model only the decay of species after an initial high level of NO and NO_2 has been generated. We, therefore, take the initial concentrations of NO and NO_2 as the peak values obtained just as the stove is shut off.

The outdoor concentrations of NO and NO_2 are obtained by interpolation of the observed outdoor concentrations taken at 5-min intervals. The infiltration/exfiltration rate R and the heterogeneous rate constants for NO and NO_2 were inferred from the data as outlined above. The heterogeneous loss terms for $O(^3P)$ and O_3 were set equal to zero in the current version, although the model can accept a nonzero heterogeneous loss term for these species. The source terms were also inferred from the data. As mentioned earlier, the values obtained for S_{NO} and S_{NO_2} agree quite well with those published in literature and those of Lawrence Berkeley Laboratory group (Traynor *et al.*, 1981) for homes with gas stoves, assuming a ratio of NO/NO_2 of 2:1. We assume no source term for $O(^3P)$ and O_3 though provision has been made for the inclusion of such terms. The chemical production and loss terms for NO and NO_2 are derived from the reaction scheme. A steady-state assumption is used for $O(^3P)$ and O_3 so that $dC/dt = 0$ for these species.

The first-order finite difference approximation allows calculation of the individual species concentrations at each time increment. We have simulated the decay curves for NO and NO_2 for two different sets of inferred parameters. The overall error for these two sets of parameters is about the same precluding any objective choice between them. Table 2 lists the parameters used in the two simulations. We may note here that an

Table 2. Inferred parameters used in chemical model (April 25/14 Simulation).[a]

Simulation	J_1	R	k_{h_1}	k_{h_2}	k_2O_3
A	0.0	0.00818	0.000908	0.0124	0.001
B	0.00304	0.00577	0.00405	0.00474	0.0

[a] All units are min^{-1}.

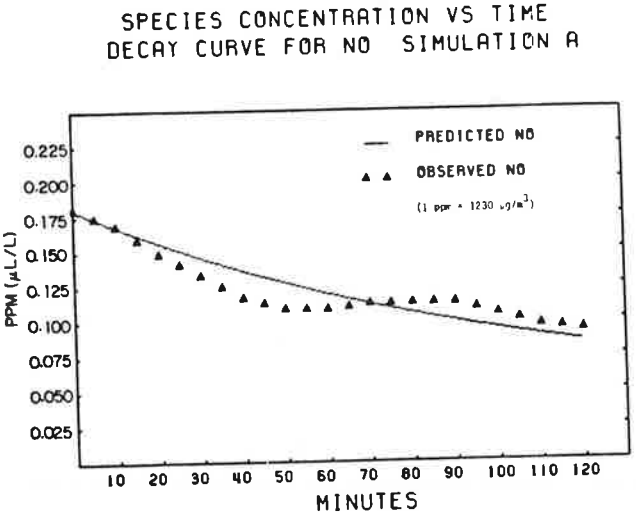

Fig. 3. Observed and predicted NO concentrations (simulation A, April 25, 1981).

explicit calculation of the ozone [as well as $O(^3P)$] concentration is made at each time step.

Figures 3 and 4 show observed and predicted decay curves for NO and NO_2 for 25 April 1981 for the first set of simulation (simulation A) parameters. Figures 5 and 6 show similar plots for the second set of simulation (simulation B) parameters. In simulation A, the photolysis rate for NO_2 is set to zero. This diminishes the effect of chemistry as the reactive odd oxygen species are then present only due to infiltration. Loss of NO_2 is effected primarily by the large heterogeneous loss rate for NO_2. The problem of mathematically separating the photolysis rate from the heterogeneous loss rate is quite evident here. Inspection of Eq. (4b) for NO_2 shows that these two terms come in multiplying the same value. Thus, the inversion procedure is effective only in predicting the sum accurately. J_1 and k_{h_2} are separable in the Eq. (4a) for NO, but this is a weaker inversion procedure than the case where it is separable in both cases. The figures for simulation A indicate the consequences of this problem. The fit of the decay curve for NO_2 is quite good, indicative of a good fit on the removal rate for this species. On the other hand, the fit for the NO decay curve is less satisfactory, due to imbalance in the chemical production scheme with a zero photolysis rate.

Simulation B gives a more balanced spread of the fitted parameters. Although the fitted value for k_2O_3 is zero, this is not used in the chemical model and thus does not eliminate the oxidation of NO to NO_2. Figures 3 and 4 for simulation B show a better fit for the decay of NO but a poorer fit for the decay of NO_2. The poor fit may be ascribed to the lower effective removal rate $(J_1 + k_h^{NO2})$ as compared with simulation A. The better fit for the decay of NO is due in part to the increase in heterogeneous loss for this species.

We present no figures here describing the time changes in $O(^3P)$ and O_3. It should be noted that in simulation A, in which there is no photolysis, the concentration of these species is fixed due to the assumption of constant infiltration rates and outdoor concentrations. In simulation B, the steady-state assumption for these species leads to very small increases in O_3 with time, with concomitant decreases in $O(^3P)$. The slopes are constant and reveal little about the reactive chemistry of the system. The concentrations are about 3×10^{-5} and 3×10^{-13} ppm (6×10^{-2} and 2×10^{-10} $\mu g/m^3$) for ozone and $O(^3P)$, respectively.

Inspection of the observed values in Figs. 3–6 show some structure in the decay curves for which our model does not account. Since we have implemented time-dependent outdoor concentrations with this model, fluctuations in outdoor concentrations cannot be postulated as being the cause for this structure. One possible cause for this missing structure in our model is the fixed nature of the photolysis, heterogeneous loss, and infiltration rates. This is most likely a good assumption

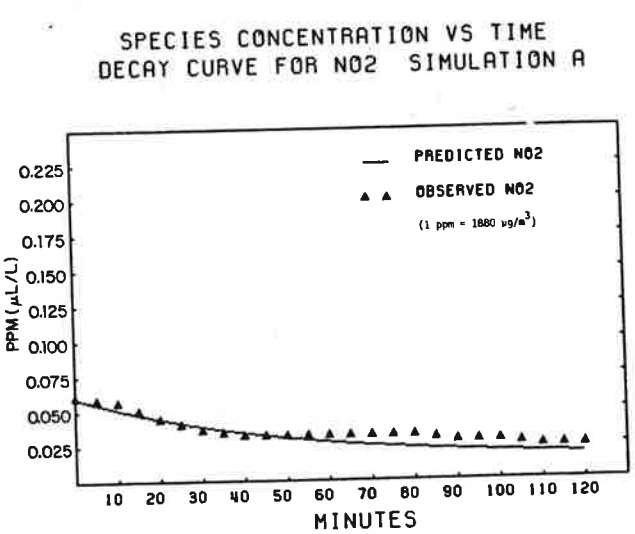

Fig. 4. Observed and predicted NO_2 concentrations (simulation A, April 25, 1981).

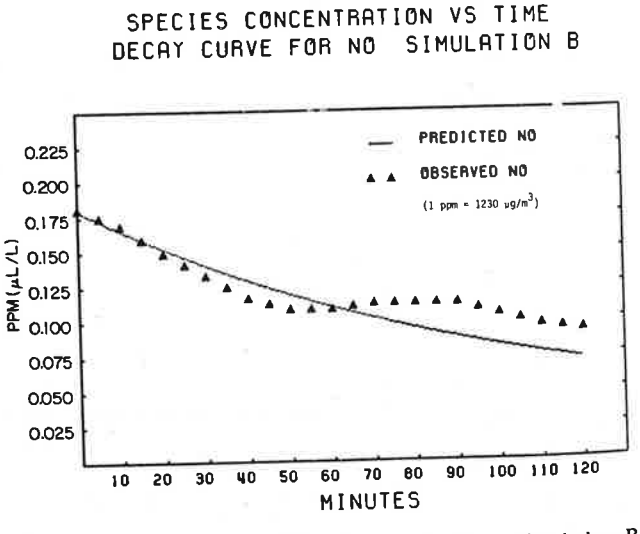

Fig. 5. Observed and predicted NO concentrations (simulation B, April 25, 1981).

8

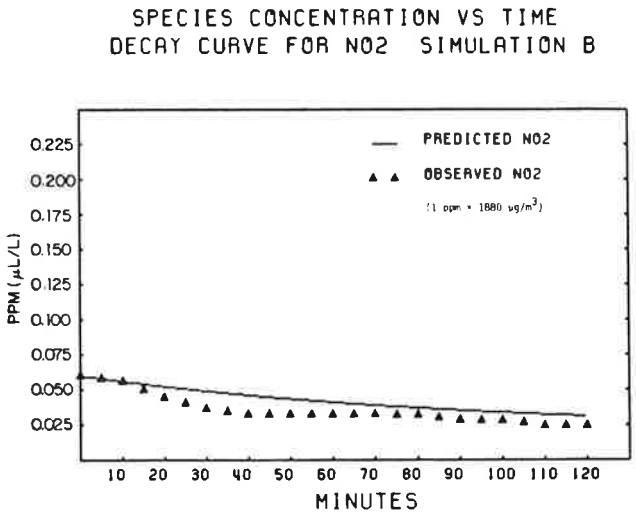

Fig. 6. Observed and predicted NO_2 concentrations (simulation B, April 25, 1981).

over the time span of the model for photolysis rates and heterogeneous loss rates. On the other hand, the infiltration rates are expected to vary with temperature differences indoors and outdoors as well as wind directions. The assumptions of (well-mixed) one-compartment reactive chemistry modeling and the choice of a single value for R over a 2-h time span may not be justified. We are currently investigating data inversions over shorter time scales as well as detailed infiltration measurements over shorter time scales.

Multicompartment simulations

To determine the mixing properties of the gases inside the kitchen, during October 1981 we conducted detailed tracer experiments during which we monitored SF_6 concentrations at various points inside the kitchen. SF_6 tracer was injected using a calibrated syringe directly over the kitchen stove. ITI Model 505 portable SF_6 Detector/Chromatograph was used manually to sample concentrations of the gas as it mixed inside the home. The four sampling positions included (measurement points chosen are shown in Fig. 2): (1) about 0.8 m above stove center, (2) about 0.4 m below ceiling and above stove, (3) kitchen center 1.5 m above floor, (4) kitchen center 0.4 m below ceiling. All the measurements were conducted by standing near the stove and moving the probe of the handheld SF_6 detector by stretching the arms from one position to another (i.e., an attempt was made to minimize as much as possible the turbulence or air currents generated by the monitoring personnel inside). There were a total of three experiments performed. Two of these were with the stove off and the other with the burners and oven on. Stove-off experiments (experiments 1 and 2) were performed after the injection of 5 and 10 cc of SF_6, respectively. Results of these tests are shown in Figs. 7 and 8. The stove-on experiment was initiated after an injection of 10 ml SF_6

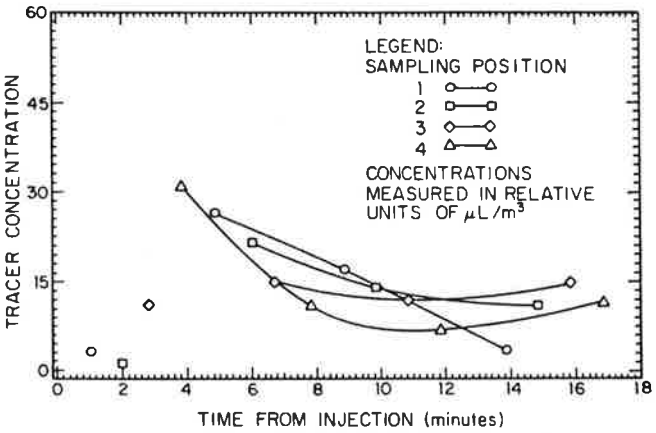

Fig. 7. Tracer measurements with stove off (experiment 1).

and after the burners and oven were on for a short period of time. Results of these measurements are presented in Fig. 9.

The main feature of all these three tracer studies is that within 2–3 min after injection the concentrations in all positions reach a peak and then decline sharply. Furthermore, a secondary rise is also noted (cf. Figs. 7 and 9) around 10 min after the injection (except in the second stove-off tracer experiment). Strong mixing patterns and the near uniformity of concentrations measured during the stove-on experiment suggests that, as expected, convection and/or thermal turbulence associated with the strong temperature gradients over the stove provide rapid mixing and flow patterns. However, as can be seen from Fig. 9, there are definitely large fluctuations in the measured concentrations within relatively short periods of time.

To be able to interpret mathematically the behavior of these large changes in the recorded tracer concentrations, we have attempted to simulate the dynamics of the mixing phenomena via two- and three-compartmental models. The basic structures of these two- and three-compartment systems were described earlier by Eq. (1) (here, however, C_o^i, P_j^i and L_j^i are all zero). Estimation of intercompartment fractional transfer coefficients (k_{ij})

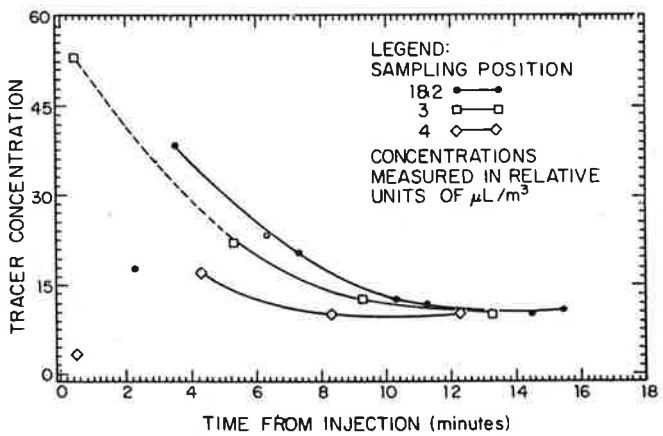

Fig. 8. Tracer measurements with stove off (experiment 2).

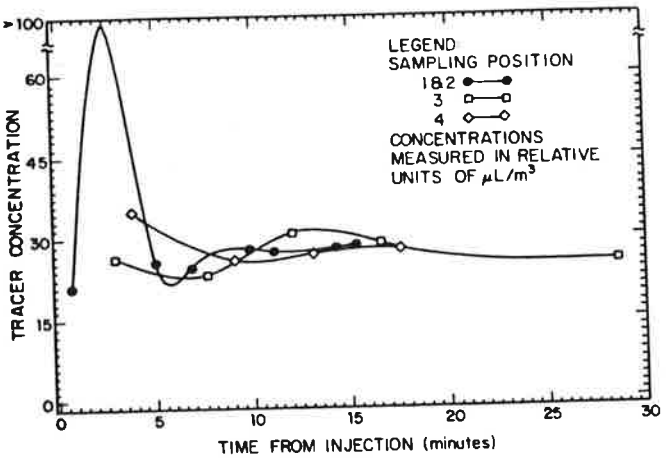

Fig. 9. Tracer measurements with stove on.

were again effected by the regularized non-negative least-squares approach discussed above. Equation (5) was solved with $\gamma = 0$ and D, A, and K defined this time by the coefficients of the linearized 2 or 3 dimensional Eq. (1). Results of these multicompartment recoveries are displayed in Tables 3 and 4. Two-compartment simulations have used the configuration A shown in Fig. 2 (i.e., position 2 and 4 results were merged to represent compartment 1's status; position 3 was used to represent compartment 2's dynamics). Three compartment simulations also used the configuration shown in Fig. 2. Here, position 1 and 2 results were combined to provide a concentration profile of the first compartment. We should also add that examination of the measurement results (cf. Figs. 7–9) were found to be supportive of this grouping of observables.

Table 3. Estimated fractional transfer coefficients (stove on).[a]

System Description	Estimated Period[b]	k_{10}	k_{12}	k_{21}	k_{20}	σ_{mn}
Two-Compartment (A)	(3–10)	3.5	2.2	2.4	0.0	2.2
Two-Compartment (A)	(10–17)	0.0	0.2	0.2	0.0	1.1

[a] Units of estimated transfer coefficients are in h^{-1}.
[b] Numerical estimation period is given in terms of elapsed time (in min) after injection of the tracer gas.

The variable σ_{mn} is the standard error of the estimate associated with the recoveries. More specifically,

$$\sigma_{mn} = \frac{\|D - A\hat{K}\|}{\sqrt{m - n}}, \tag{7}$$

where $\hat{K}$ = the vector of inferred transfer coefficients;
m, n = the dimensions of matrix A ($m = 30$, $n = 9$ for two-compartment model; $m = 45$, $n = 9$ for three-compartment model);
D = the data vector of time rate of change of SF_6 concentrations at positions studied;
A = the coefficient matrix (kernel) formed from Eq. (1).

As noted from Tables 3 and 4 the goodness of fit varies over time. In general, nearer the injection (within 3–5 min) or around the secondary rise (or more accurately, during altered mixing conditions), σ_{mn} is larger than those obtained at other periods. A choice of the three-compartment model over the two-compartment model may not yet be made objectively (based on σ_{mn} values at least). However, more physical insight into mixing and flow conditions are definitely obtained by the three-compartment model.

Estimates shown in Table 4 point to the existence of an interesting and perhaps organized mixing pattern. The two open doorways on each side of the kitchen clearly provide natural pathways for the exchange of hot and cold air between the kitchen and the rest of the house. Thus, the nature of special flow patterns due to input of cold air (near the floor level) and the output of warm air (near the ceiling) also contribute to the establishment of the vertical temperature structure in the kitchen together with its associated buoyancy effects. Three-compartment stove-on studies point to the fact that initially (3–6.5 min) there is rapid dispersion and transfer from the source compartment into others, including to outside the kitchen (either to the rest of the house or outdoors). After this period, the tracer that has buoyantly risen in large quantities near the ceiling starts

Table 4. Estimated fractional transfer coefficients.[a]

System Description	Estimation Period[b]	k_{10}	k_{12}	k_{13}	k_{21}	k_{23}	k_{20}	k_{31}	k_{32}	k_{30}	σ_{mn}
Three-Compartment/Stove On	(3–6.5)	11.1	6.8	6.8	8.8	0.0	1.6	5.9	0.7	3.9	3.0
Three-Compartment/Stove On	(6.5–10)	0.0	0.8	0.0	0.0	0.0	0.0	1.9	0.6	0.0	0.9
Three-Compartment/Stove On	(10–13.5)	0.0	1.2	0.0	0.5	0.6	0.0	0.1	0.9	0.0	1.2
Three-Compartment/Stove On	(13.5–17)	0.1	0.0	0.2	0.2	0.5	0.3	0.0	0.0	0.0	0.2
Three-Compartment/Stove On	(3–10)	4.9	8.3	4.3	11.8	0.0	0.0	1.8	2.1	3.6	2.8
Three-Compartment/Stove On	(10–17)	0.0	2.9	0.0	1.7	1.1	0.0	0.9	0.0	0.0	0.8
Three-Compartment/Stove Off[c]	(3–10)	10.4	0.0	0.0	0.5	0.0	8.4	1.4	1.1	7.4	1.8
Three-Compartment/Stove Off	(10–17)	1.1	0.1	0.4	0.0	0.2	0.9	0.0	0.0	0.7	0.3

[a] Units of estimated transfer coefficients are in h^{-1}.
[b] Numerical estimation period is given in terms of elapsed time (in min) after the injection of the tracer gas.
[c] Corresponds to second tracer experiment with burners and oven off.

mixing to compartment 2 and also back into compartment 1. After 10 min, the effect of turbulent eddies and/or circular flow patterns inside the kitchen become more prominent during the development of steady-state tracer concentrations inside the kitchen. For example, after 13.5 min the tracer mixed into compartment 2 along with warm air from the stove (which is typically higher in temperature than the surrounding air near the floor) is forced to rise upward (from compartment 2 to 3 and from 2 to 1 and then to 3) as well as move outward. Seven-minute recoveries obtained by the two-compartment data inversions approximate these observations as well. Stove-off simulation (experiment 2) indicates more outward transfers (i.e., decay) than internal mixing patterns. Although experiment 1 with the stove off has not yet been simulated, Fig. 7 suggests complex internal mixing patterns as found for the stove-on case represented by the results shown in Fig. 9 and Table 4.

Further tracer or other types of dispersion experiments to resolve and characterize these observations better (within sharper spatial and temporal scales) would be needed to test the implication of these findings on the potential variability of personal exposures to indoor pollutants within homes. Finally, it seems also quite promising to expand such multicompartmental models by incorporating appropriate reactive chemistry within each compartment to model indoor air quality.

Conclusions

We have developed and tested one- and multicompartmental models to infer and estimate concentration, emission, removal, ventilation, and transfer (mixing) related variables pertinent to modeling indoor air quality. The simple reactive chemistry model developed during this study accounts for most of the essential features of the NO_x chemistry in our indoor environment. Furthermore, this model (along with others) can be generalized to account for more chemical reactions and in multicompartments with relative ease since the data inferral procedure allows us to find effective removal (deposition/reaction) rates for these species.

Based on our investigations, it can be concluded that the short-term ($\leq$ 10–15 min) air flow and mixing patterns may be important in controlling pollutant concentrations and thus potential exposure characteristics within homes with gas cooking stoves.

Finally, it should again be pointed out that the results discussed in this paper represent findings for a single dwelling over limited simulation time spans. Therefore further studies, involving (1) simultaneous measurements of NO, NO_2, O_3, and key hydrocarbon species (both indoors and outdoors), (2) detailed tracer, dispersion, and filtration measurements, and (3) measurement of temperature differences and wind speed/wind direction, are needed to characterize concentration/exposure patterns in homes in an accurate manner.

Acknowledgements— Portions of this work were supported by NIEHS Grant ES-01108; Electric Power Research Institute RP-1001; EPA 68-02-3201 and 2794; and U.S. Department of Energy DE-AC02-81EV10731. We gratefully acknowledge Dr. John D. Spengler (Harvard University) for his expert guidance and steady encouragement, Dr. David T. Mage (EPA) for many helpful discussions, David W. Bearg (Life Energy Associates) for conducting the tracer measurements, and Debra L. Swanson (Harvard University) for her support during computer programming and in the preparation of this manuscript.

References

AER (1981) Study of the role of transport in fine and total suspended particulate air quality. NTIS pub. PB81-168031, AER report prepared for the NCAQ, Washington, DC.

Bottenheim, J. W. and Strausz, O. P. (1980) Gas-phase chemistry of clean air at 55° latitude, *Environ. Sci. Technol.* **14**, 709–718.

Grot, R. A. (1979) A low-cost method for measuring air infiltration rates in a large sample of dwellings. NBSIR 79-1728, April 1979, National Bureau of Standards, Washington, DC.

Lawson, C. L. and Hanson, R. J. (1974) *Solving Least Squares Problems*. Prentice-Hall, Inc., Englewood Cliffs, NJ.

National Academy of Science (1981) *Indoor Pollutants*. Committee on Indoor Pollutants. National Academy Press, Washington, DC.

Özkaynak, H., Ryan, P. B., and Bosart, L. F. (1982) Modeling of pollutant transport and removal during a regional sulfate episode, *Water Air Soil Pollut.* **18**, 157–171.

Tikhonov, A. N. (1963) Regularization of incorrectly posed problems, *Sov. Math. Dokl.* **4**, 1624–1627.

Traynor, G. W., Apte, M. G., Girman, J. R., and Hollowell, C. D. (1981) Indoor air pollution from domestic combustion appliances. Report No. LBL-12886, Lawrence Berkeley Laboratory, Berkeley, CA.

Whitten, G. Z., Hogo, H., and Killus, J. P. (1980) The carbon-bond mechanism for photochemical smog, *Environ. Sci. Technol.* **14**, 690–700.

Williams, M. D., Treiman, E., and Wecksung, M. (1980) Plume blight visibility modeling with a simulated photograph technique, *J. Air Pollut. Control Assoc.* **30**, 131–134.